Theoretical investigation of superconductivity in $SrAuSi_3$ and $SrAu_2Si_2$

Enes Arslan[a], Ertuğrul Karaca[a], H. M. Tütüncü[a,b], A. Başoglu[a,b] and G. P. Srivastava[c]

[a] *Sakarya Üniversitesi, Fen-Edebiyat Fakültesi, Fizik Bölümü, 54187, Adapazarı, Turkey*

[b] *Sakarya Üniversitesi, BIMAYAM Biyomedikal, Manyetik ve Yarıiletken Malzemeler Araştırma Merkezi, 54187, Sakarya , Turkey*

[b] *School of Physics, University of Exeter, Stocker Road, Exeter EX4 4QL, UK*

Abstract

The structural and electronic properties of $BaNiSn_3$-type $SrAuSi_3$ and $ThCr_2Si_2$-type $SrAu_2Si_2$ have been investigated by using the planewave pseudopotential method and the density functional theory. The electronic structures and phonon dispersion relations of these two materials have been analyzed with and without the inclusion of spin-orbit interaction, and similarities and differences highlighted. By integrating the Eliashberg spectral function $\alpha^2F(\omega)$, the average electron-phonon coupling parameter is determined to be $\lambda = 0.47$ for $SrAuSi_3$ and 0.42 for $SrAu_2Si_2$. The largest contribution to the electron-phonon coupling for $SrAuSi_3$ comes from the Si p electrons near the Fermi energy and Si-related vibrations. Using a reasonable value of $\mu^* = 0.12$ for the effective Coulomb repulsion parameter, the superconducting critical temperature T_c for $SrAuSi_3$ is found to be 1.47 K which compares very well with its experimental value of 1.54 K.

Key words: A.silicides; B.density functional theory,electronic structure, superconducting properties; E. abinitio calculations,physical properties;

1 Introduction

Since the discovery of pressure-induced superconductivity in $CeRhSi_3$ [1] and $CeIrSi_3$ [2], a significant number of experimental and theoretical investigations have been per-

[1] Corresponding Author: H. M. Tütüncü Tel: +90 264 295 60 72 Fax: +90 264 295 59 50 e-Mail: tutuncu@sakarya.edu.tr

formed on isostructural intermetallics crystallizing in body-centered tetragonal $BaNiSn_3$-type unit cells (space group I4mm). The main reason for these studies is to describe the role of the noncentrosymmetric crystal structure in the formation of unconventional Cooper pairing with nodes in the superconducting gap. Several Ce materials [1–16] crystallizing in $BaNiSn_3$-type structure have been found to be superconductors, and show interesting physical properties. The majority of Ce materials are antiferromagnetic and become superconducting only under pressure. However, in materials such as $BaPtSi_3$ [17], $LaRhSi_3$ [18], $CaPtSi_3$ [19,20], $CaIrSi_3$ [19,20], $LaPtSi_3$ [21], and $LaPdSi_3$ [21], which also adopt the body-centered tetragonal $BaNiSn_3$-type structure but do not show strong electronic correlations, superconductivity with the BCS characteristics has been discovered at ambient pressure.

On the theoretical side, electronic, vibrational and superconducting properties of $BaPtSi_3$ [17] have been investigated by using the density functional theory within the local density approximation. This theoretical work [17] reveals that the overall effect of noninversion symmetry plays a minor role for superconducting properties of this material. The electronic properties of $CaIrSi_3$ and $CaPtSi_3$ have been studied using the density functional theory within a generalized gradient approximation [22]. This work indicates that the electronic structures of these materials exhibit similarities to that of $BaPtSi_3$ [17] and further clarifies that all them behave in a very similar way. The electronic structure of $LaPdSi_3$, a superconductor without inversion symmetry, and its non-superconducting counterpart $LaPdGe_3$, have been studied using the full-potential local-orbital method (FPLO) within the density functional theory [23]. This work shows that spin-orbit interaction for both materials has only negligible effect on the band structure around the Fermi energy.

A recent experiment shows that $SrAuSi_3$ [24], which also has the body-centered tetragonal $BaNiSn_3$-type structure, exhibits superconductivity with a critical temperature (T_c) of 1.54 K. This material is the first reported noncentrosymmetric superconductor that contains Au as a principal constituent element [24]. The electronic properties of $SrAuSi_3$ have been studied by means of the full-potential linearized augmented plane wave (FLAPW) employing a generalized gradient approximation of the density functional theory [24]. The spin-orbit interaction is included as a perturbation to the scalar-relativistic equations. This theoretical work [24] reveals that the spin-orbit interaction for this superconductor has only negligible effect on the band structure around the Fermi energy. Moreover, this theoretical work [24] shows that the band structure around the Fermi energy is dominated by Si p states and the mechanism of superconductivity is suggested as phonon induced. This theoretical work also presents the electronic properties of $SrAu_2Si_2$. Different from $SrAuSi_3$, $SrAu_2Si_2$ exists in the body-centered tetragonal $ThCr_2Si_2$ structure [25], with space group I4/mmm. This structure and the common $BaNiSn_3$ structures are both derivatives of the $BaAl_4$-type structure [26]. $ThCr_2Si_2$-type AM_2X_2 compounds (A: an alkaline earth or a lanthanide element; M: a transition metal; X: P, Ge, or As) have also been widely studied due to their superconducting and magnetic properties [27–34]. Recently, the lattice parameters, electronic structures, elastic constants, Vicker's hardness and thermodynamics properties of $SrAuSi_3$ were systematically investigated by using first-principles and the quasi-harmonic Debye model [35]. In this

theoretical work [35], the superconducting transition temperature (T_c) for $SrAuSi_3$ is calculated to be 9.94 K which is much larger than its experimental value of 1.54 K [24].

Despite detailed studies of the electronic properties of $SrAuSi_3$ and $SrAu_2Si_2$, no experimental or theoretical results have been made to determine electron-phonon interaction in these materials. It is firmly believed that the electron-phonon interaction controls a number of interesting properties of solids, including the electrical and thermal resistivites, superconductivity, renormalization of low temperature electronic component of the heat capacity, and a number of other physical properties. With this in mind, in this work, we have investigated the structural and electronic properties of $SrAuSi_3$ and $SrAu_2Si_2$ using the *ab initio* pseudo-potential method based on a generalized gradient approximation of the density functional theory [36]. The calculated lattice and internal parameters for both materials are compared with their experimental values [24,25]. Details of the electronic band structure and the electronic density of states near the Fermi energy are presented and discussed. Furthermore, the dynamical properties of $SrAuSi_3$ and $SrAu_2Si_2$ have been investigated using a linear response theory [36]. The phonon dispersion curves and the phonon density of states for these materials are compared with each other in detail. Finally, electron-phonon matrix elements for both materials are calculated using the linear response method [36] and the Migdal-Eliashberg approach [37,38]. The phonon dispersion relations and the electron-phonon matrix elements are then used to determine the Eliashberg spectral function [37–42], from which the electron-phonon coupling parameter is calculated. Finally, the superconducting parameters for both materials are presented and compared with each other, and an explanation has been made for observed differences.

2 Method

All first-principles calculations in this work are carried out using the ultrasoft pseudopotential [43] plane-wave method within the framework of density functional theory (DFT) as implemented in the QUANTUM ESPRESSO package [36]. The exchange-correlation effects are treated within the generalized gradient approximation (GGA) in the scheme of Perdrew–Burke–Ernzerhof (PBE) [44]. The Kohn–Sham [45] wave functions of valence electrons are expanded by a plane-wave basis set within the kinetic energy cutoff of 60 Ry. The self-consistent procedure for total energy calculations is performed on the 8×8×8 grid of $\boldsymbol{k}$-points uniformly distributed in the irreducible part of the Brillouin zone (BZ) using the Monkhorst-Pack scheme [46]. The electronic structure and the electronic density of states have been determined with the (24×24×24) grid. Although previous theoretical calculations [24] show that the spin-orbit interaction has only negligible effect on the band structure around the Fermi energy, in our study calculations were made with and without the inclusion of spin-orbit interaction for Au and Si atoms.

Phonon calculations has been made by means of the density-functional perturbation theory (DFPT) [36]. The self-consistent procedure for phonon calculations is performed on the 8×8×8 grid of $\boldsymbol{k}$-points uniformly distributed in the irreducible part of the Brillouin zone (BZ) using the Monkhorst-Pack scheme [46]. Within the DFPT, the second-order derivatives of the total energy such as the dynamical matrices are obtained from the static linear response of the electrons to the difference of the external potential due to periodic displacements of the atoms. The response of the electrons is taken into account iteratively, until self-consistency is acquired between the variation of the charge density and the screened perturbing potential. In order to obtain complete phonon dispersion curves, we calculate the dynamical matrices at a grid of thirteen uniformly distributed points corresponding to a (444) mesh for the body-centered tetragonal lattice. The dynamical matrices at arbitrary wave vectors are evaluated with the help of a Fourier deconvolution on this mesh.

The linear response method [36,41,42] and Migdal-Eliashberg theory [37–40] have been used to calculate the electron-phonon coupling matrix, the average electron-phonon coupling parameter (λ) and the superconducting transition temperature (T_c). According to this theory, T_c depends on the effective screened Coulomb repulsion constant (μ^*) and the Eliashberg spectral function ($\alpha^2F(\omega)$). The function α^2F(ω) is formed by two important factors, α^2 and ($F(\omega)$). The second term is similar to the phonon density of states while the first one contains an average square of the electron-phonon matrix element. The calculation of the Eliashberg spectral function ($\alpha^2F(\omega)$) has been done using a very fine ($24 \times 24 \times 24$) $\boldsymbol{k}$ points mesh in performing the Fermi surface average of the electron-phonon matrix elements. The electron-phonon mass enhancement parameter λ is given as [41,42]

$$\lambda = 2\int_0^\infty \mathrm{d}\omega \frac{\alpha^2 F(\omega)}{\omega}. \tag{1}$$

The superconducting transition temperature T_c can be calculated on the basis of the Allen-Dynes [39,40] modification of the McMillan formula [47],

$$T_c = \frac{\omega_{\ln}}{1.2}\exp\left(-\frac{1.04(1+\lambda)}{\lambda - \mu^*(1+0.62\lambda)}\right), \tag{2}$$

where ω_{ln} shows the logarithmically averaged frequency and the screened Coulomb pseudopotential parameter (μ^*) takes a value between 0.10 and 0.20 [40]. Finally, the logarithmically averaged frequency (ω_{ln}) can be calculated from

$$\omega_{ln} = exp\left(2\lambda^{-1}\int_0^\infty \frac{\mathrm{d}\omega}{\omega}\alpha^2 F(\omega) ln\omega\right). \tag{3}$$

3 Results

3.1 Structural and Electronic Properties

The tetragonal crystal structure of $SrAuSi_3$ (space group symmetry I4mm) is shown in Fig. 1(a). The atoms inside a unit cell can be categorized as four nonequivalent crystallographic sites: Sr, Au, Si1, and Si2 according to the symmetry. The atomic positions are: Sr (2a) (0, 0, 0), Au (2a) (0, 0, z_{Au}), Si1 (2a) (0, 0, z_{Si1}), and Si2 (4b) (0,1/2,z_{Si1}), (1/2, 0, z_{Si2}). Here, z_{Au}, z_{Si1} and z_{Si2} are the internal parameters. In the $SrAuSi_3$ crystal, the Au atom is surrounded by four basal Si2 atoms and one apical Si1 atom. The values of the Au-Si1 and Au-Si2 bond lengths are calculated to be 2.543 $\mathring{A}$ and 2.550 $\mathring{A}$, respectively, which compare very well with their experimental values of 2.493 $\mathring{A}$ and 2.543 $\mathring{A}$ [24]. The value of the Si1-Si2 bond length is found to be 2.529 $\mathring{A}$ which is slightly smaller than the corresponding value of 2.352 $\mathring{A}$ in the diamond Si.

The body-centered tetragonal $ThCr_2Si_2$ structure (space group I4/mmm) of $SrAu_2Si_2$ is show in Fig. 1(b). Different from the crystal structure of $SrAuSi_3$, this structure has only one crystallographic site for each atomic types and one internal parameter z_{si} which designates the relative position of Si within in the unit cell. In the $SrAu_2Si_2$ structure, atomic positions are Sr (2a) (0, 0,0), Au (4d) (0,1/2,1/4), (1/2, 0, 1/4), and Si (4e) (0, 0, z_{Si}), (0, 0, -z_{Si}). Different from the crystal structure of $SrAuSi_3$, the crystal structure of $SrAu_2Si_2$ is formed by three parameters: two lattice constants (a and c) and one internal parameter z_{Si}. The crystal structure of $SrAu_2Si_2$ contains negatively charged Au_2Si_2 and positively charged Sr layers. Thus, the bonding between Sr and Au-Si layers has mainly the ionic character, but in the Au-Si layer there is a sign of not only covalent Au-Si character but also of some metallic character. The bond length between Si atoms of the adjacent Si-Au-Si layers is found to be 2.378 $\mathring{A}$, which is close to the corresponding value of 2.352 $\mathring{A}$ in the diamond Si. This result suggests that there is a strong covalent Si-Si bond between adjacent layers. The $BaNiSn_3$ structure of $SrAuSi_3$ and the $ThCr_2Si_2$ structure of $SrAu_2Si_2$ are both derivatives of the $BaAl_4$-type structure. The Sr atoms occupy identical positions in both structures and generate a body-centered tetragonal lattice. The atomic layer stacking in these two structures is as follows: SiAuSi-SiAuSi in $SrAu_2Si_2$ and AuSiSi-AuSiSi in $SrAuSi_3$. Thus, stacking order of Au and Si layers along the c axis is different in these two structures. $SrAuSi_3$ has neither the mirror plane perpendicular to the c-axis nor the inversion center for the unit structure.

To begin with, we performed the total energy calculations to determine the equilibrium structural parameters for $SrAuSi_3$ and $SrAu_2Si_2$. Then, around the region of the total energy minimum, the bulk modulus, the pressure coefficient B' and the equilibrium volume were obtained by fitting numerical data to Murnaghan's equation of state [48]. The calculated structural parameters together with available experimental [25,24,35] and theoretical [35] results are presented in Tab. 1. The calculated lattice parameters and internal parameters for both structures are in acceptable agreement with their corresponding experimental values [25,24]. To the best of our

knowledge, there are no experimental results for the values of B and B$'$. However, the calculated values of B and B$'$ can be compared with previous GGA values of 91.5 GPa and 4.59 [35].

The electronic structure and electronic density of states for $SrAuSi_3$ are illustrated in Fig. 2. The overall band profiles are found to be in good accordance with the previous GGA results [24,35]. The electronic structure of $SrAuSi_3$ shows the metallic character of this material since at least one band cuts the Fermi level along all the considered symmetry directions. The valence bands of this material are constituted by five regions of electronic states mixing: -11.90 eV to -9.5 eV, -9.5 eV to -6.6 eV, -6.6 to -5.0 eV, -5.0 to -3.0 eV and -3.0 to 0.0 eV. From -11.90 to 9.5 eV, the DOS features are mostly contributed by Si(1,2) s and p states with smaller contributions from Sr 5p and Au 6p states. From -9.5 to -6.6 eV, the DOS features are mainly derived from Si(1,2) s and p and Au 5d states with lesser contribution from Sr 4d states. From -6.6 to -5.0 eV, the DOS features are primarily dominated by Au 5d states with admixture of Si(1,2) p states. Hybridized states between Au and Si(1,2) atoms are primarily concentrated in the energy interval of -5.0 to -3.0 eV which correspond to the strong covalent Au-Si bonds in $SrAuSi_3$. Finally, from -3.0 to the Fermi level, the DOS features are primarily dominated by Si(1,2) p states with some contributions from Au 5d, Au 6p and Sr 4d states. We have to note that the contributions from the valence states of Sr to the occupied bands of $SrAuSi_3$ is small because Sr atoms in this material are in the charge states near to Sr^{2+}. Thus, Sr atomic sheets and the Au-Si blocks are connected between each other by ionic interactions. Since electrons near the Fermi level govern the superconducting properties of solids, it is necessary to find out their nature. For $SrAuSi_3$, without the inclusion of spin-orbit coupling (SOC) the density of states at the Fermi level ($N(E_F)$) is calculated to be 1.41 States/eV, which is larger than the previous GGA value of 1.30 States/eV [24]. We think that this difference is due to the difference in the atomic geometry used in the two calculations: we have used structurally optimized parameters from our GGA electronic calculations, while Isobe and co-workers [24] have used experimental structural parameters for their GGA electronic calculations. As we have mentioned before, the most interesting difference between $SrAuSi_3$ and $SrAu_2Si_2$ relates the inversion center for symmetry: $SrAuSi_3$ has neither the mirror plane perpendicular to the z-axis nor the inversion center for the unit cell structure. With this in mind, we have calculated the value of $N(E_F)$ using full relativistic ultrasoft pseudopotentials including the relativistic effect of the spin-orbit coupling (SOC). The value of $N(E_F)$ with SOC is found to be 1.39 States/eV which is close to the corresponding value of 1.41 States/eV without SOC. This result confirms that the effect of SOC for $SrAuSi_3$ in a small energy window around the Fermi level is rather small. We have to mention that a similar observation has been made in the previous GGA work of Isobe and co-workers [24]. The contributions of Sr, Au, Si1, Si2 to $N(E_F)$ are approximately 12%, 18%, 25% and 45%. In particular, the total contribution of Si(1,2) p states to $N(E_F)$ is approximately 60%. This results signs that the p electrons of Si atoms have main effects on the superconducting properties of $SrAuSi_3$ since Cooper pairs in the BSC theory are generated by electrons which have energies close to the Fermi level. Above the Fermi level, the DOS features are derived from Sr 4d and Sr(1,2) p states.

The electronic band structure and electronic density of states for $SrAu_2Si_2$ are displayed in Fig. 3. Again, some bands cross the Fermi level, confirming the metallic nature of this material. In agreement with $SrAuSi_3$, the partial DOS of Au and Si are widely scattered in the energy region below as well as above the Fermi level. The two lowest lying bands in the energy region from -10.9 to -7.4 eV arise mainly from Si 3s orbitals with admixture of other electronic states. Different from $SrAuSi_3$, these lower valence bands are separated by a forbidden gap of 0.5 eV from the higher valance bands which lie from -6.9 eV to the Fermi level. From -6.9 to -2.7 eV, the DOS features contain mainly d contributions from Au 5d states with a lesser contribution from Si 3p band electrons. The valance bands (located in the range from -2.7 eV to the Fermi level) are formed predominantly mixed Au 5d and Si 3p states, which are responsible for the covalent bonding inside $[Au_2Si_2]$ blocks. The density of states at the Fermi level ($N(E_F)$) for $SrAu_2Si_2$ amounts to be 1.59 States/eV which is larger than the corresponding value of 1.41 States/eV for $SrAuSi_3$. The orbital analysis of the DOS reveals that primarily Sr (19%), Au (36%) and Si (45%) electronic states are contributing to $N(E_F)$. From the above results, we can conclude that the contribution of Au atoms to $N(E_F)$ for $SrAu_2Si_2$ increases as compared to the corresponding contribution for $SrAuSi_3$. This change can be related to the number of Au atoms in the primitive unit cells of $SrAu_2Si_2$ and $SrAuSi_3$. The primitive unit cell of $SrAuSi_3$ contains one Au atom while the primitive unit cell of $SrAu_2Si_2$ includes two Au atoms. Due to similar reason, the contribution of Si atoms to $N(E_F)$ for $SrAu_2Si_2$ decrease as compared to the corresponding contribution for $SrAuSi_3$.

3.2 Phonons and Electron-Phonon interaction

The zone-center phonons for $SrAuSi_3$ and $SrAu_2Si_2$ can be categorized by the irreducible representations of the point groups c_{4v} and D_{4h}, respectively. Accordingly, the symmetries of the optical phonon modes for $SrAuSi_3$ and $SrAu_2Si_2$ can be expressed as:

$$\Gamma(SrAuSi_3) = 4E + 3A_1 + B_2,$$
$$\Gamma(SrAu_2Si_2) = B_{1g} + 2E_g + E_u + 2A_u + A_g,$$

with the B, A and E modes being singly, singly and doubly degenerate, respectively. A comparison of the zone-center phonon frequencies and their electron-phonon coupling parameters for $SrAuSi_3$ and $SrAu_2Si_2$ are given in Tab. 2. We have also included our SOC results for $SrAuSi_3$ in this table. This table clearly shows that the effect of SOC on the phonon frequencies and their electron-phonon coupling parameter is very small. Thus, we will present our phononic and electron-phonon interactions results without SOC. It is important to note that the doubly degenerate E modes for both materials are characterized by the vibrations of the related atoms in the **x** and **y** plane, whereas the A and B modes come from the vibrations of related atoms along the **z** axis. It can be seen from a critical assessment of Tab. 2 for $SrAuSi_3$ that all the zone-center optical phonon modes have negligible electron-phonon coupling parameter except for the B_2 and the highest A_1 phonon modes. The electron-phonon coupling parameters of these phonon modes are calculated to 0.144 and 0.205, respectively. Fig. 4(a) illustrates the eigenvector representations of

these phonon modes. Both these phonon modes contain Si-related vibrations. The B_2 phonon mode is characterized by the opposing motion of Si2 atoms along the **z** direction. For the highest A_1 phonon mode, Si1 atoms vibrate against Si2 atoms along the the **z** direction. From these two pictures, it can be naively expected that the strong vibrations of Si1 and Si2 atoms may bring about strong electron-phonon interaction due to the considerable contribution of Si(1,2) p electrons at the Fermi level.

For $SrAu_2Si_2$, strong electron-phonon interaction has been predicted for the lowest and highest optical phonon modes, with the values of 0.261 and 0.165, respectively. The eigenvector representations of these phonon modes are shown in Fig. 4(b). The lowest B_{1g} phonon mode corresponds to the opposing motions of Au atoms along the **z** direction while the highest A_{1g} mode results from the opposing vibrations of Si atoms along the **z** direction. The eigenvector representations of these phonon modes give rise to the overlap of Si and Au electronic states. This overlap leads to larger electron-phonon coupling parameter for these phonons mode than other zone-centre phonon modes. This result is not surprising for us because the density of states at the Fermi level for $SrAu_2Si_2$ is dominated by the Si and Au electronic states. Thus, Si-related and Au-related vibrational phonon modes together with the Si 3p, Au 5d and Au 6p states may generate the superconducting properties of $SrAu_2Si_2$. This is in contrast to the situation for $SrAuSi_3$, which is governed by Si-related vibrational modes and Si(1,2) p states.

The calculated phonon dispersion curves along high-symmetry lines in the body-centered tetragonal Brillouin zone (BZ) and the atomic projected phonon density of states (PDOS) for $SrAuSi_3$ are displayed in Fig. 5. In the phonon spectrum of all the fifteen phonon branches extends up to 10.5 THz. The calculated phonon dispersion curves have positive frequencies at any wave vector, indicating the dynamical stability of $SrAuSi_3$ in the body-centered tetragonal $BaNiSn_3$-type structure. The peaks at 1.96 and 2.56 THz in the PDOS are due to the flatness of transverse acoustic (TA) branches and longitudinal acoustic branch close to the zone boundaries. The first peak at 1.96 THz is formed by a strong Au-Si hybridization with a much smaller contribution from Sr atoms. The sharpest peak at 2.56 THz is composed of nearly Au vibrations with smaller contributions from remaining atoms. The Sr-related phonons located in the low-frequency region are primarily confined to the frequency region from 2.8 to 3.5 THz. Smaller Si and Au contributions have been observed in this frequency region. Si as the lightest element in this material dominates at the high frequency region above 3.5 THz. The partial density of states of Au and Sr atoms are negligible in this part of the spectrum. Finally, the Si-related phonon densities partake in lattice vibrations over the whole range of phonon frequencies while the partial DOS of Si electronic states are widely scattered in the energy region below as well as above the Fermi level. This observation may confirm that Si p states and Si-related phonon modes are crucial for superconductivity in $SrAuSi_3$.

Fig. 6 shows the phonon dispersion curves of $SrAu_2Si_2$ along different symmetry directions of the body-centered tetragonal Brillouin zone and the corresponding total and atom-projected density of states. Again, the dynamical stability of $SrAu_2Si_2$ is

confirmed by the lack of any imaginary frequency modes in the whole BZ. However, the total phonon spectrum of $SrAu_2Si_2$ has an frequency rage of 11.50 THz which is 1.0 THz larger than the corresponding value of 10.50 THz for $SrAuSi_3$. This is probably due to the strong covalent Si-Si bond between adjacent layers in $SrAu_2Si_2$. We also note that the phonon spectrum of $SrAu_2Si_2$ is quite different from that of $SrAuSi_3$. Different from $SrAuSi_3$, there are three forbidden gaps in the phonon dispersion curves of $SrAu_2Si_2$. The frequencies of these gaps are found to be about 0.4, 1.8 and 3.0 THz, respectively. Due to these forbidden gaps, the phonon dispersion curves for $SrAu_2Si_2$ split into four distinct regions: low-frequency band (LFB) (0-2.6 THz), second frequency band (SFB)(3.0-4.0 THz), third frequency band (TFB) (5.8-7.9 THz) and high frequency band (HFB) (10.90-11.50 THz). The LFB is formed by three acoustic and three weakly dispersive optical phonon branches. The most noteworthy feature in the LFB is that there is remarkable overlap between the acoustic and optical phonon branches. This suggests that the heat-carrying acoustic branches can potentially be scattered by the low-lying optical phonon branches, which may result in comparatively lower thermal conductivity of $SrAu_2Si_2$. The SFB consists of three optical phonon branches while there are five strongly dispersive optical phonon branches in the TFB. The highest optical branch in the HFB is weakly dispersive compared to five optical phonon branches in the TFB. In the LFB, the phonon density of states show that Au atoms dominate the vibrations with a minor contribution from Si and Sr atoms. The sharp peak at 1.8 THz in this frequency region is due to the flatness of low-lying optical phonon branches. The Sr-related phonons are primarily confined to the SFB. The TFB is totally characterized by the vibrations of Si atoms while the remaining atoms are stationary. The peak at 11.0 THz in the HFB contains mainly pure Si-Si bond-stretching characteristics, showing the picture of strongly bonded Si dimer for $SrAu_2Si_2$.

The main target of this *ab-initio* work is to research the strengths of the electron-phonon interaction in $SrAuSi_3$ and $SrAu_2Si_2$ in order to better find out the presence of superconductivity in these compounds. In order to do this, we have illustrated the calculated Eliashberg spectral function ($\alpha^2F(\omega)$) and the average electron-phonon coupling parameter (λ) together in Fig. 7. The numerical results for λ are found to be 0.47 and 0.42 for $SrAuSi_3$ and $SrAu_2Si_2$, respectively, which signals that the electron-phonon interactions in both these materials is of weak strength. In addition to this, we can conclude that the electron-phonon interaction in $SrAuSi_3$ is slightly stronger than the corresponding interaction in $SrAu_2Si_2$.

Now, we point out the connection between phonon modes and their electron-phonon coupling parameters by analyzing the calculated Eliashberg spectral function ($\alpha^2F(\omega)$) for $SrAuSi_3$. The phonon modes below 2.8 THz contribute approximately 29% (0.136) to λ. This contribution is not surprising because phonon modes in this frequency region are due the coupled motion of Au and Si atoms. Both atoms make a considerable contribution to the density of states at the Fermi level. Sr-related phonon modes in the frequency range from 2.8 to 3.5 THz contribute about 1% (0.047). This result suggests that the motion of Sr atoms play a relatively trivial role in forming the superconducting state of $SrAuSi_3$ due to the insignificant presence of Sr electronic states at the Fermi level. The largest contribution to λ comes from

Si-related phonon modes above 3.5 THz within approximately 70%(0.287) because of the considerable existence the Si p electrons at the Fermi level. Thus, we can conclude that Si-related phonon modes are more involved in the process of scattering of electrons than other phonon modes.

We now analyze the spectral contribution to λ for $SrAu_2Si_2$. In the frequency region below 2.6 THz, we observe that the value of λ grows rapidly with increasing frequency. The largest contribution to λ comes from the phonon modes in this region within approximately 54%(0.227). The Au-related phonon modes with smaller contribution from Si vibrations exist in this frequency region and Au electronic states make a large contribution to $N(E_F)$. The contribution of phonon bands between 3.0 and 4.0 THz to λ is about 7%(0.029). This contribution is admissible because Sr-related phonon modes exist in this frequency region and the smallest contribution to $N(E_F)$ arises from Sr electronic states. Si-related phonon modes above 5.8 THz make a noteworthy contribution, about 39%(0.164). Thus, we can conclude that the motion of Au and Si atoms play a important role in determining the superconducting properties of $SrAu_2Si_2$.

The superconducting transition temperature T_c for $SrAuSi_3$ and $SrAu_2Si_2$ can be determined from the Allan-Dynes modification of the McMillian formula (see Eq. 2) [40]. Using Eq.3, the value of logarithmically averaged frequency ω_{ln} is found to be 235.81 K for $SrAuSi_3$ and 156.98 K for $SrAu_2Si_2$. Using the Allan-Dynes modification of the McMillian formula for T_c and taking a typical value of μ^*=0.12, the value of the superconducting transition temperature is predicted to be 1.47 K for $SrAuSi_3$ and 0.57 K for $SrAu_2Si_2$. The calculated value of T_c for $SrAuSi_3$ is in excellent accordance with its experimental value of 1.54 K [24]. The calculated value of T_c for $SrAuSi_3$ is considerably larger than the corresponding value for $SrAu_2Si_2$. According to the Allan-Dynes modification of the McMillian formula, the logarithmically averaged frequency and the average electron-phonon coupling parameter can effect the T_c values of superconductors. The values of both parameters for $SrAuSi_3$ are larger than those for $SrAu_2Si_2$, making the T_c value of $SrAuSi_3$ higher.

4 Summary and Conclusion

In summary, the structural and electronic properties for the body-centered tetragonal $SrAuSi_3$ and $SrAu_2Si_2$ have been investigated using the density-functional theory within the generalized gradient approximation. Our calculated structural parameters for both materials are in good accordance with available experimental results. The electronic band structures of both materials demonstrate that they are both metals. The bonding nature in both materials is a combination of metallic, covalent and ionic bonds. Further analysis of the electronic density of states for $SrAuSi_3$ indicates that the electronic bands near the Fermi level are dominated by Si(1,2) p states with smaller contribution from other electronic states. However, energy bands near the Fermi level for $SrAu_2Si_2$ originate from Si p and Au (p and d) orbitals. The effect of spin-orbit interaction (SOC) is found to be minimal in determining the value of

the electronic density of states at the Fermi level ($N(E_F)$) as well as the zone-center phonon mode energies.

Our phonon calculations show that the optimized structures of $SrAuSi_3$ and $SrAu_2Si_2$ are both dynamically stable. However, the phonon spectrum of $SrAu_2Si_2$ is very different from that of $SrAuSi_3$. First, the width of the phonon spectrum of $SrAu_2Si_2$ is 1.0 THz larger than that of $SrAuSi_3$. This is probably due to the strong covalent Si-Si bond between adjacent layers in $SrAu_2Si_2$. Secondly, the phonon spectrum of $SrAu_2Si_2$ can be divided into four distinct regions while there is no clear phonon band gap in the phonon spectrum of $SrAuSi_3$. Thirdly, there is considerable overlap between the acoustic and optical modes in the phonon dispersion curves of $SrAu_2Si_2$. Finally, the low frequency phonon modes in $SrAuSi_3$ are due the coupled motion of Si and Au atoms while these phonon modes in $SrAu_2Si_2$ are mainly dominated by the vibrations of Au atoms.

A comparison of the shape of the Eliashberg spectral function and that of phonon density of states for $SrAuSi_3$ shows that the Si-related phonon modes are more involved in the process of scattering of electrons than other phonon modes. This result is expected because the density of states at the Fermi level for this material is mainly composed of Si(1,2) p orbitals. However, a detailed examination of the Eliashberg spectral function for $SrAu_2Si_2$ reveals that the acoustic and low-frequency optical phonon branches due to the vibrations of Au atoms make a large contribution within around 54% to average electron-phonon coupling parameter λ. This results is also expected since the contribution of Au electronic state to $N(E_F)$ for $SrAu_2Si_2$ is much larger than the corresponding contribution to $N(E_F)$ for $SrAuSi_3$. However, Sr-related phonon modes play a relatively unimportant role in obtaining the superconducting properties of both materials because of the insignificant presence of the Sr electronic states at the Fermi energy. For $SrAuSi_3$, the value of average electron-phonon coupling parameter λ is 0.47, and the superconducting critical temperature is estimated to be 1.47 K, in excellent accordance with experimental value of 1.54 K. Our calculated superconducting parameters for $SrAu_2Si_2$ reveal that the electron-phonon interaction in this material is slightly weaker than the corresponding interaction in $SrAuSi_3$. Thus, the value of superconducting critical temperature for $SrAu_2Si_2$ is predicted to be 0.57 K which much lower than the corresponding value of 1.54 K for $SrAuSi_3$.

ACKNOWLEDGEMENT

This work was supported by the Scientific and Technical Research Council of Turkey (TÜBİTAK) (Project Number MFAG-115F135).

References

[1] N. Kimura, K. Ito, K. Saitoh, Y. Umeda, H. Aoki, and T. Terashima, Phys. Rev. Lett. 95 (2005) 247004.

[2] I. Sugitani, Y. Okuda, H. Shishido, T. Yamada, A. Thamizhavel, E. Yamamoto, T. D. Matsuda, Y. Haga, T. Takeuchi, R. Settai, and Y. Önuki, J. Phys. Soc. Jpn. 75 (2006) 043703.

[3] Y. Okuda, Y. Miyauchi, Y. Ida, Y. Takeda, C. Tonohiro, Y. Oduchi, T. Yamada, N. D. Dung, T. D. Matsuda, Y. Haga, T. Takeuchi, M. Hagiwara, K. Kindo, H. Harima, K. Sugiyama, R. Settai, and Y. Y. Önuki, J. Phys. Soc. Jpn. 76 (2007) 044708.

[4] N. Kimura, Y. Muro, and H. Aoki, J. Phys. Soc. Jpn. 76 (2007) 051010.

[5] N. Aso, H. Miyano, H. Yoshizawa, N. Kimura, T. Komatsubara, and H. Aoki, J. Magn. Magn. Mater. 310 (2007) 602.

[6] R. Settai, T. Takeuchi, and Y. Y. Önuki, J. Phys. Soc. Jpn. 76 (2007) 051003.

[7] F. Tomioka, M. Hedo, I. Umehara, T. Ono, Y. Uwatoko, N. Kimura, and S. Takayanagi, J. Magn. Magn. Mater. 310 (2007) 340.

[8] Y. Muro, M. Ishikawa, K Hirota, Z. Hiroi, N. Takeda, N. Kimura, and H. Aoki, J. Phys. Soc. Jpn. 76 (2007) 033706.

[9] T. Shimoda, Y. Okuda, Y. Takeda, Y. Iida, Y. Miyauchi, T. Kawai, T. Fujie, I. Sugitane, A. Thamizhavel, T. D. Matsuda, Y. Haga, T. Takeuchi, M. Nakashimad, R. Settai, and Y. Y. Önuki, J. Magn. Magn. Mater. 310 (2007) 308.

[10] T. Terashima, Y. Takahide, T. Matsumoto, S. Uji, N. Kimura, H. Aoki, and H. Harima, Phys. Rev. B 76 (2007) 054507.

[11] T. Kawai, H. Muranaka, M. A. Measson, T. Shimoda, Y. Doi, T. D. Matsuda, Y. Haga, G. Knebel, G. Lapertot, D. Aoki, J. Flouquet, T. Takeuchi, R. Settai, and Y. Önuki, J. Phys. Soc. Jpn. 77 (2008) 064716.

[12] R. Settai, Y. Miyauchi, T. Takeuchi, F. Levy, I. Sheikin, and Y. Önuki, J. Phys. Soc. Jpn. 77 (2008) 073705.

[13] T. Ohkochi, T. Toshimitsu, H. Yamagami, S. Fujimori, A. Yasui, Y. Takeda, T. Okane, Y. Saitoh, A. Fujimori, Y. Miyauchi, Y. Okuda, R. Settai, and Y. Önuki, J. Phys. Soc. Jpn. 78 (2009) 084802.

[14] H. Mukuda, T. Ohara, M. Yashima, Y. Kitaoka, R. Settai, Y. Önuki, K. M. Itoh, and E. E. Haller, Phys. Rev. Lett. 104 (2010) 017002.

[15] R. Settai, K. Katayama, D. Aoki, I. Sheikin, G. Knebel, J. Flouquet, and Y. Önuki, J. Phys. Soc. Jpn. 80 (2011) 094703.

[16] N. Aso, M. Takahashi, H. Yoshizawa, H. Iida, N. Kimura, and H. Aoki, J. Phys. Soc. Jpn. 80 (2011) 095004.

[17] E. Bauer, R. T. Khan, H. Michor ,E.Royanian, A. Grytsiv, N. Melnychenko-Koblyuk, P. Rogl, R. Reith, R. Podloucky, E.-W. Scheidt, W. Wolf, and M. Marsman, Phys. Rev. B 80 (2009) 064504.

[18] V. K. Anand, A. D. Hillier, D. T. Adroja, A. M. Strydom, H. Michor, K. A. McEwen, and B. D. Rainford, Phys. Rev. B 83 (2011) 064522.

[19] G. Eguchi, D. C. Peets, M. Kriener, Y. Maeno, E. Nishibori, Y. Kumazawa, K. Banno, S. Maki, and H. Sawa, Phys. Rev. B 83 (2011) 024512.

[20] R. P. Singh, A. D. Hillier, D. Chowdhury, J. A. T. Barker, D. McK. Paul, M. R. Lees, and G. Balakrishnan, Phys. Rev. B 90 (2014) 104504.

[21] M. Smidman, A. D. Hillier, D. T. Adroja, M. R. Lees, V. K. Anand, R. P. Singh, R. I. Smith, D. M. Paul, and G. Balakrishnan, Phys. Rev. B 89 (2014) 094509.

[22] J. Kaczkowski, and A. Jezierski, J. Alloy. Compd. 509 (2011) 6142.

[23] M. J. Winiarski and M. Samsel-Czekala, Intermetallics 56 (2015) 44.

[24] M. Isobe, H. Yoshida, K. Kimoto, M. Arai, and E. Takayama-Muromachi, Chem. Matter. 26 (2014) 2155.

[25] W. Dörrscheidt, N. Niess, and H. Z. Schäfer, Naturforsch. B 31 (1976) 890.

[26] E. Parthe, B. Chabot, H. F. Braun, and N.Engel, Acta Crystallogr. B 39 (1983) 588.

[27] W. Jeitschko, R. Glaum, and L. Boonk, J. Solid State Chem. 69 (1987) 93.

[28] M. Reehuis, W. Jeitschko, M. H. Moller, and P. J. Brown, J. Phys. Chem. Solids 53 (1992) 687.

[29] J. An, A. S. Sefat, D. J. Singh, and M. H. Du, Phys. Rev. B 79 (2009) 075120.

[30] N. H. Sung, J. S. Rhyee, and B. K. Cho, Phys. Rev. B 83 (2011) 094511.

[31] J. W. Wang, I. A. Chen, T. L. Hung, Y. B. You, H. C. Ku, Y. Y. Hsu, J. C. Ho and Y. Y. Chen, Phys. Rev. B 85 (2012) 024538.

[32] T. L. Hung, I. A. Chen, C. H. Huang, C. Y. Lin, C. W. Chen, Y. B. You, S. T. Jian, M. C. Yang, Y. Y. Hsu, J. C. Ho, Y. Y. Chen, and H. C. Ku, J. Low Temp Phys 171 (2013) 148.

[33] T. Samuely, J. G. Rodrigo, N. H. Sung, B. K. Cho, and P. Samuely, J. Supercond. Nov. Magn. 26 (2013) 1199.

[34] V. K. Anand, H. Kim, M. A. Tanatar, R. Prozorov, and D. C. Johnston, Phys. Rev. B 87 (2013) 224510.

[35] C. Shu, J. Long, S. Li, and W. Yang, J. Alloy. Compd. 650 (2015) 553.

[36] P. Giannozzi, S. Baroni, N. Bonini, M. Calandra, R. Car, C. Cavazzoni, D. Ceresoli, G. L. Chiarotti, M. Cococcioni, I. Dabo, A.D. Corso, S. de Gironcoli, S. Fabris, G. Fratesi, R. Gebauer, U. Gerstmann, C. Gougoussis, A. Kokalj, M. Lazzeri, L. Martin-Samos, N. Marzari, F. Mauri, R. Mazzarello, S. Paolini, A. Pasquarello, L. Paulatto, C. Sbraccia, S. Scandolo, G. Sclauzero, A.P. Seitsonen, A. Smogunov, P. Umari and R.M. Wentzcovitch, J. Phys.: Condens. Matter 21 (2009) 395502.

[37] A.B. Migdal, Zh. Eksp. Teor. Fiz. 34 (1958) 1438.

[38] G.M. Eliashberg, Sov. Phys. JETP. 11 (1960) 696.

[39] P. B. Allen, Phys. Rev. B 6 (1972) 2577.

[40] P. B. Allen and R. C. Dynes, Phys. Rev. B 12 (1975) 905.

[41] R. Bauer, A. Schmid, P. Pavone, and D. Strauch, Phys. Rev. B 57 (1998) 11276.

[42] S. Bağcı, H. M. Tütüncü, S. Duman, and G. P. Srivastava, Phys. Rev. B 81 (2010) 144507.

[43] A. M. Rappe, K. M. Rabe, E. Kaxiras, and J. D. Joannopoulos, Phys. Rev. B 41 (1990) 1227.

[44] J. P. Perdew, K. Burke, and M. Erzerhof, Phys. Rev. Lett. 77 (1996) 3865.

[45] W. Kohn and L. J. Sham, Phys. Rev. 140 (1965) A1133.

[46] H. J. Monkhorst and J. D. Pack, Phys. Rev. B 13 (1976) 5188.

[47] W. L. McMillian, Phys. Rev. B 167 (1968) 331.

[48] F. D. Murnaghan, Proc. Nat. Acad. Sci. USA 50 (1944) 697.

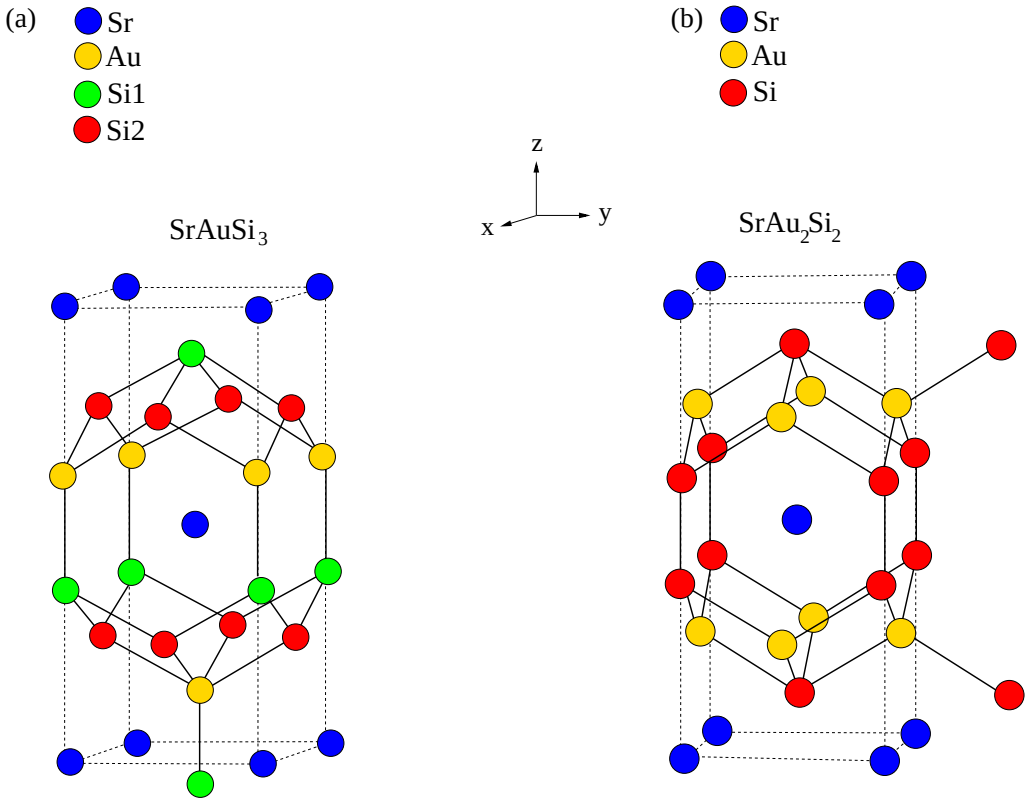

Fig. 1. (a) The $BaNiSn_3$ crystal structure of $SrAuSi_3$. (b) The $ThCr_2Si_2$ crystal structure of $SrAu_2Si_2$.

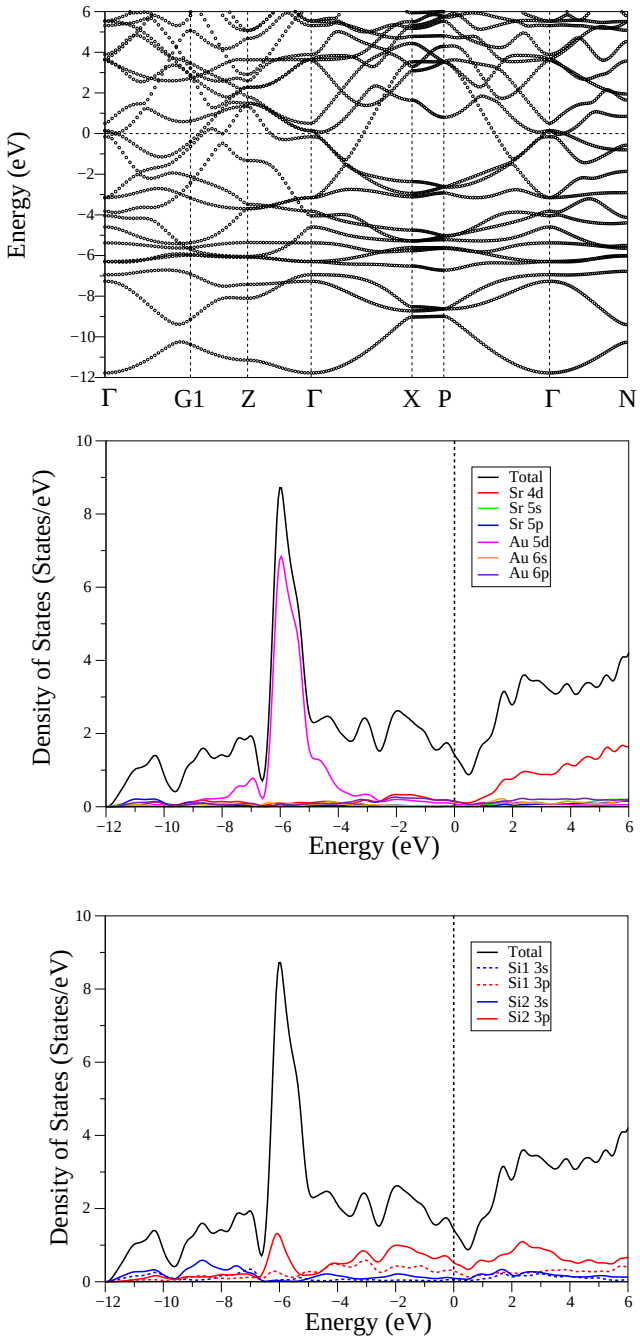

Fig. 2. The electronic band structure and electronic density of states for $SrAuSi_3$ in the $BaNiSn_3$ crystal structure. The Fermi level corresponds to 0 eV. The high-symmetry points in the irreducible Brillouin zone in cartesian coordinates are: G1= $\frac{2\pi}{a}((\frac{1}{2}+\frac{a^2}{2c^2})$, 0.00, 0.00), Z = $\frac{2\pi}{a}$(0.00,0.00,$\frac{a}{c}$), X= $\frac{2\pi}{a}$(0.50,0.50,0.00), P= $\frac{2\pi}{a}$(0.50,0.50,$\frac{a}{2c}$), and N= $\frac{2\pi}{a}$(0.0,0.50,$\frac{a}{2c}$). Note that G1 is the zone boundary in the [100] direction.

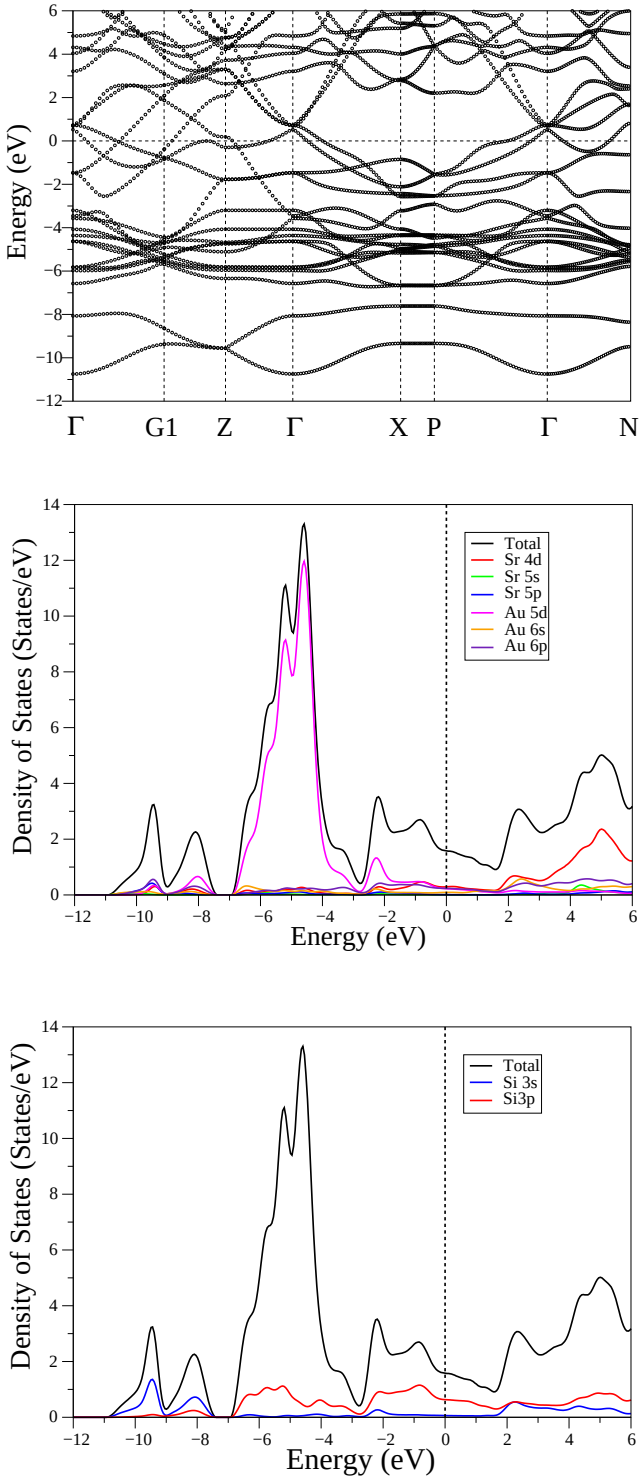

Fig. 3. The electronic band structure and electronic density of states for $SrAu_2Si_2$ in the $ThCr_2Si_2$ crystal structure. The Fermi level corresponds to 0 eV.

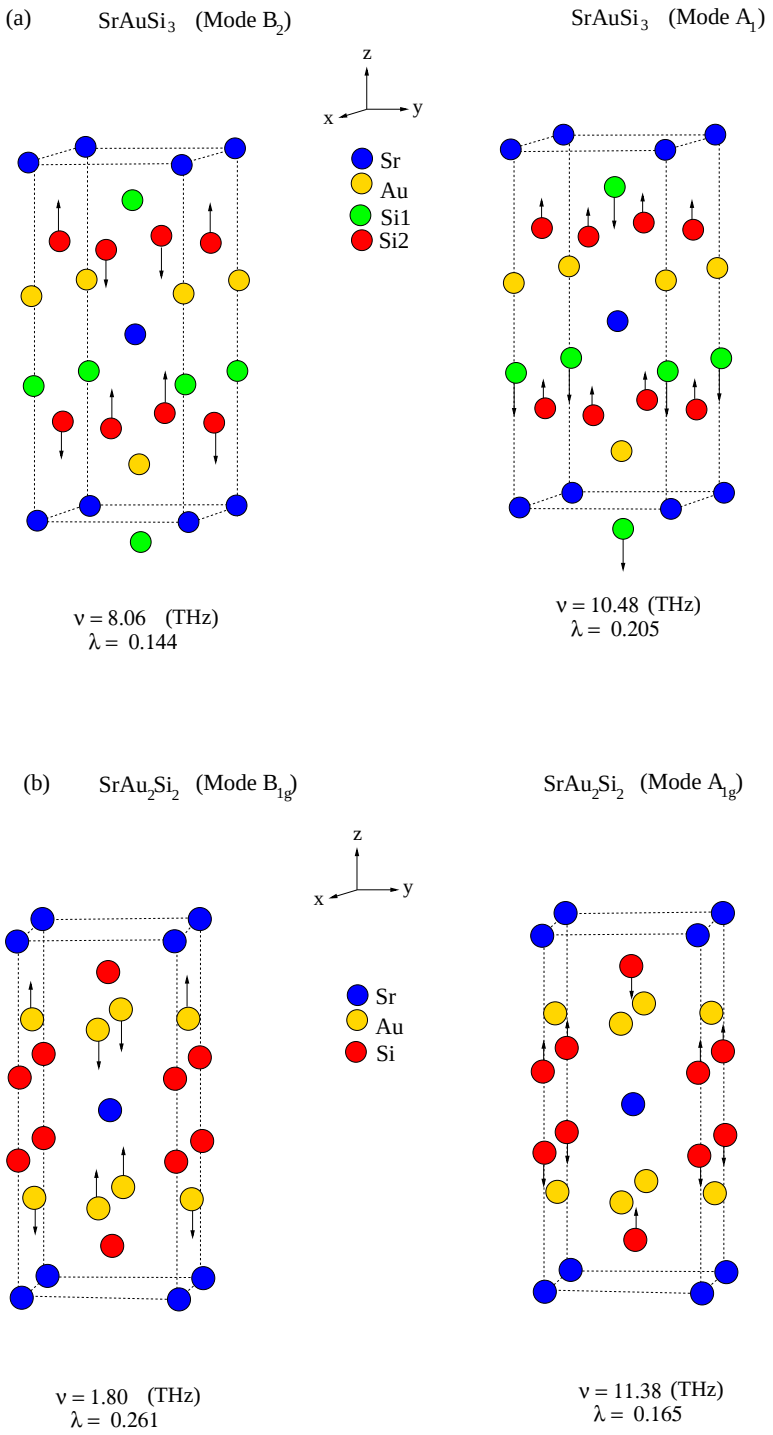

Fig. 4. (a) Eigenvector representations of the zone-centre B_2 and A_1 phonon modes in $SrAuSi_3$ (b) Eigenvector representations of the zone-centre B_{1g} and A_{1g} phonon modes in $SrAu_2Si_2$.

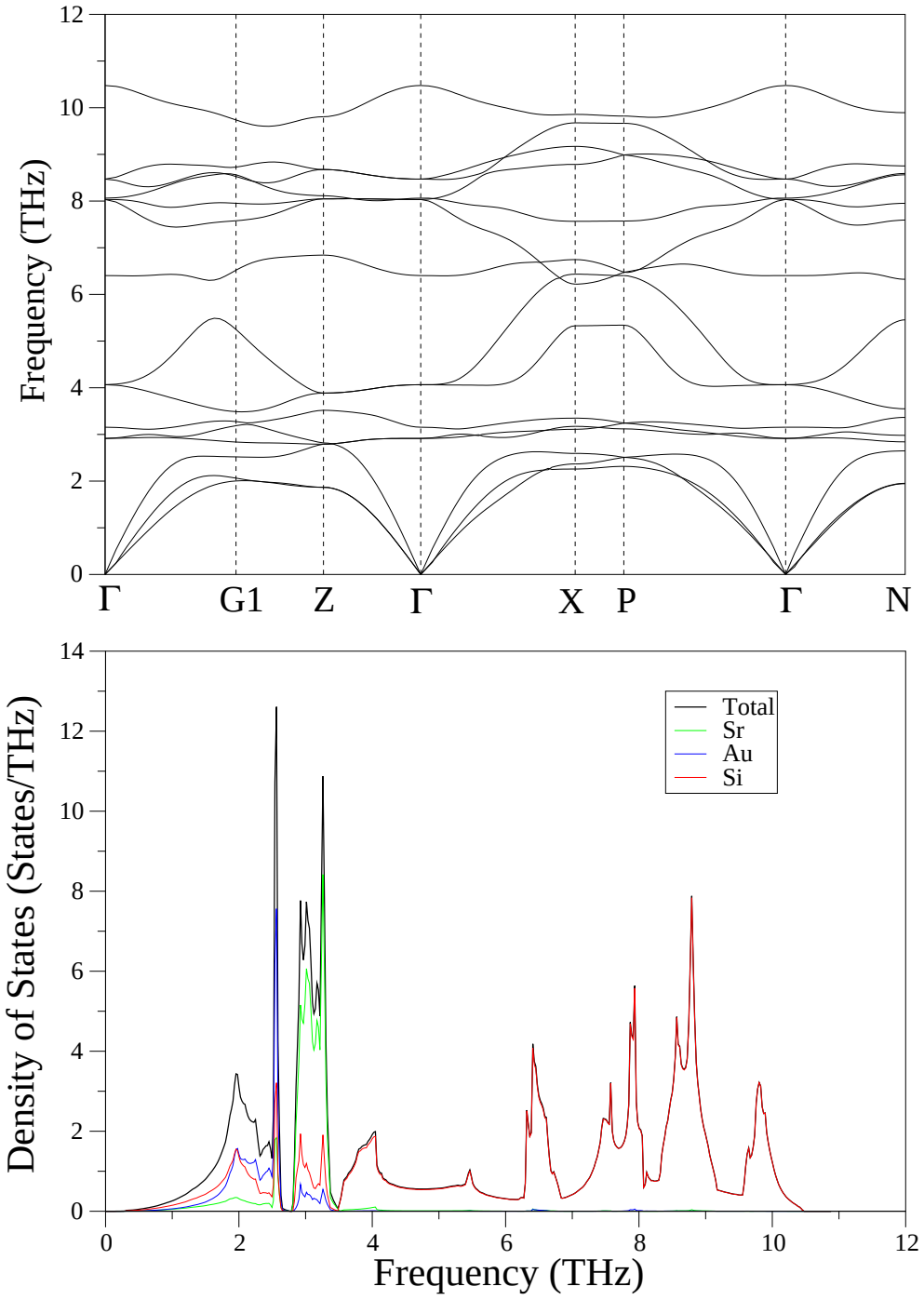

Fig. 5. The phonon band structure and phonon density of states for $SrAuSi_3$ in the $BaNiSn_3$ crystal structure.

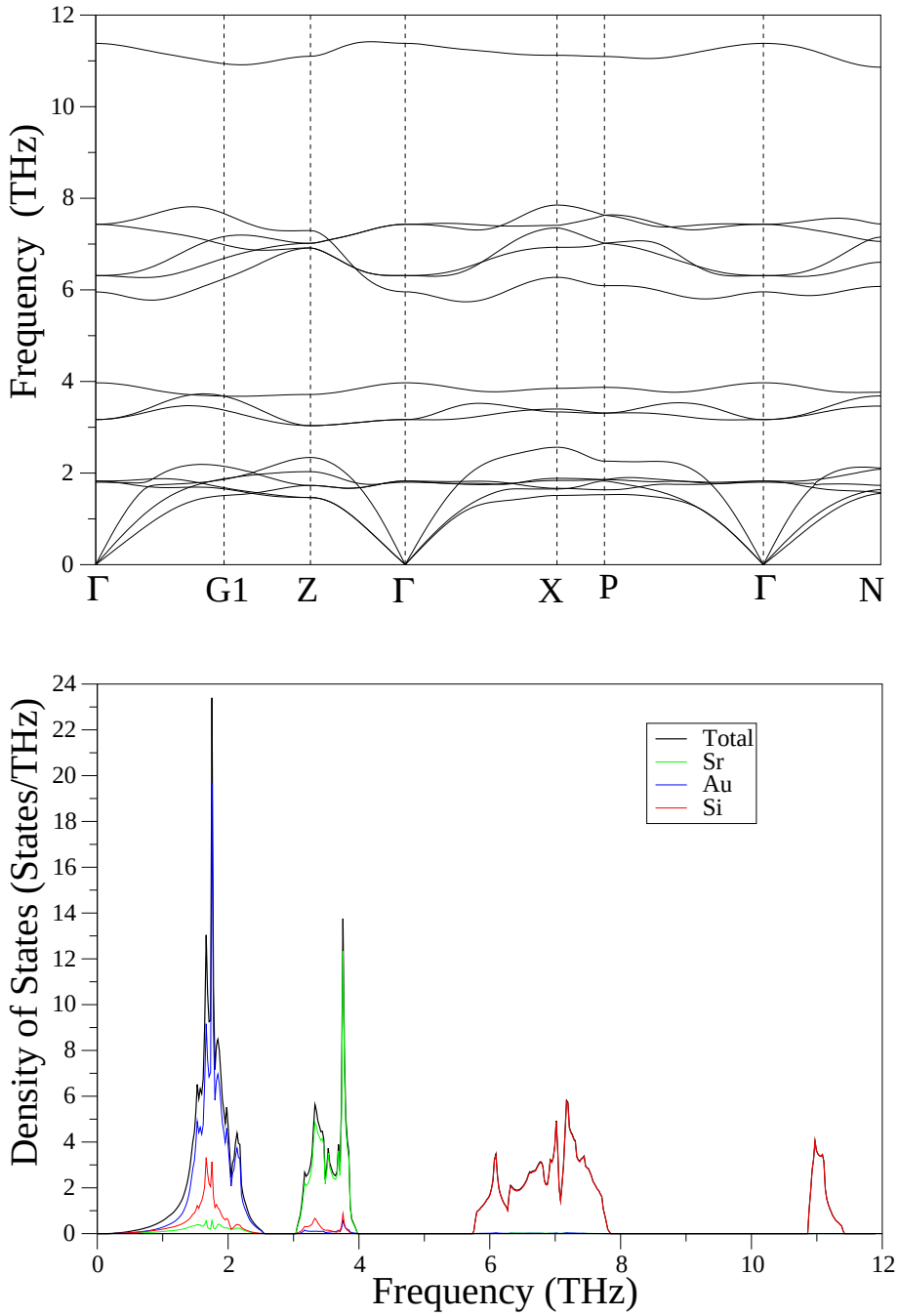

Fig. 6. The phonon band structure and phonon density of states for $SrAu_2Si_2$ in the $ThCr_2Si_2$ crystal structure.

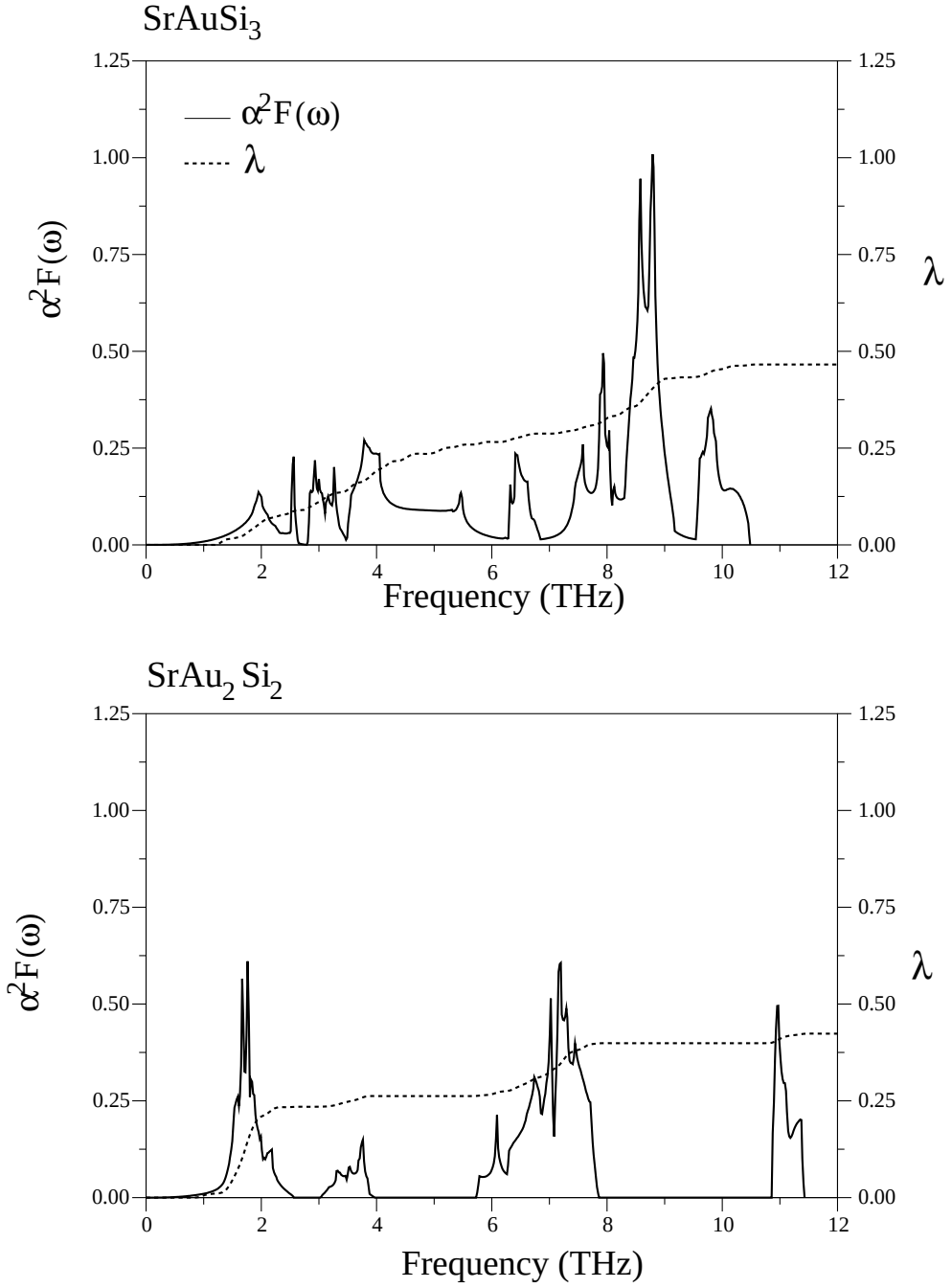

Fig. 7. The calculated electron-phonon spectral function α^2F(ω) (solid line) and the variation of the electron-phonon coupling parameter (dashed line) with rising frequency for $SrAuSi_3$ and $SrAu_2Si_2$

Table 1
Structural parameters for the body-centered tetragonal $SrAuSi_3$ and $SrAu_2Si_2$ and their comparison with experimental results.

$SrAuSi_3$								
Source	$a(\AA)$	$c(\AA)$	V($\AA^3$)	z_{Au}	z_{Si1}	z_{Si2}	B(GPa)	B$'$
This work	4.475	10.136	101.506	0.632	0.378	0.257	81.70	4.68
Experimental [24]	4.409	9.947	96.681	0.629	0.378	0.258		
GGA [35]	4.405	9.929	96.331				91.5	4.59
$SrAu_2Si_2$								
Source	$a(\AA)$	$c(\AA)$	V($\AA^3$)		z_{Si}		B(GPa)	B$'$
This work	4.472	10.128	101.230		0.382		85.70	5.00
Experimental [25]	4.370	10.144	96.821		0.363			

Table 2
Calculated frequencies of zone-center phonon modes (ν in THz) and the electron-phonon coupling parameters for $SrAuSi_3$ and $SrAu_2Si_2$. The calculated results for $SrAuSi_3$ with the inclusion of spin-orbit coupling (SOC) also presented. R and IR indicate Raman-active and infrared-active vibrations, respectively.

$SrAuSi_3$								
Mode	E	A_1	E	A_1	E	B_2	E	A_1
ν without SOC	2.92	3.16	4.07	6.40	8.03	8.06	8.47	10.48
ν with SOC	2.94	3.15	4.10	6.38	7.99	8.01	8.49	10.42
λ without SOC	0.032	0.055	0.037	0.040	0.026	0.140	0.061	0.205
λ with SOC	0.030	0.050	0.033	0.037	0.025	0.130	0.060	0.198
Active	IR+R	IR+R	IR+R	IR+R	IR+R	R	IR+R	IR+R
$SrAu_2Si_2$								
Mode	B_{1g}	E_g	E_u	A_{2u}	A_{2u}	E_u	E_g	A_{1g}
ν (in THz)	1.80	1.83	3.18	3.97	5.96	6.31	7.43	11.38
λ	0.261	0.058	0.001	0.003	0.004	0.004	0.025	0.165
Active	R	R	IR	IR	IR	IR	R	R